"On-The-Fly" Fabrication of Highly-Ordered Interconnected Cylindrical and Spherical Porous Microparticles *via* Dual Polymerization Zone Microfluidics

Shahriar Sajjadi[*1], *Mohammad Alroaithi*[2], *Ankur S. Chaurasia*[3], *and Fatemeh Jahanzad*[4]

[1] Faculty of Natural and Mathematical Sciences, King's College London, Strand, London, WC2R 2LS, UK.
[2] Research Development Center, Saudi Aramco, Thuwal 23955-6900, Kingdom of Saudi Arabia
[3] ESPCI Paris, 10 Rue Vauquelin, 75231, Paris cedex 05, Paris, France
[4] Division of Chemical and Petroleum Engineering, London South Bank University, London, SE1, UK.

ABSTRACT

A microfluidic platform with dual photopolymerization zones has been developed for production of novel uniform interconnected porous particles with shapes imposed either by the geometry of the external capillary or by the thermodynamic minimisation of interfacial area. Double w/o/w drops with well-defined internal droplet size and number were produced and then exposed to online photopolymerization to create the porous particles. Cylindrical interconnected porous particles were produced in a segmented flow where the drops took the shape of the capillary. The microfluidic set up included an extension capillary where the drops relaxed and conformed to their thermodynamically favoured morphology. Window opening of the particles occurred "on-the-fly" during UV polymerization without using any offline auxiliary methods. A distinction was made between critically and highly packed arrangements in double drops. The window opening occurred consistently for highly packed spherical drops, but only for critically packed drops containing more than 6 internal cores at internal phase ratio as low as 0.35. The size and number of cores, shape and structure of double drops could be precisely tuned by the flowrate and by packing structure of the inner droplets.

* **Corresponding Author**

Faculty of Natural and Mathematical Sciences, Kings College London, Strand, London, WC2R 2LS, UK. Email: Shahriar-sajjadi-emami@kcl.ac.uk; Telephone number: +44-(0)20 7848 2322.

INTRODUCTION

Porous materials have already been estabished as interesting area of research due to their distinctive permeable structure within a polymer matrix. They are characterised by the presence of pores with a wide range of sizes usually within 2-50 nm, and enjoy several advantages over impermeable substances, including light weight, a network of well-connected pores, high surface area and excellent absorption capacity.[1,2,3] Porous polymeric particles, which are miniature porous entities, are increasingly becoming an interesting area of research due to their smaller size and increased permeability. They have attracted enormous applications including ion exchange resin[4], separation and filtration[5], encapsulation agents for controlled release of drugs[6], catalysts[7] or supports for catalysts[8], and packing materials in chromatography industries.[9,10,11,12] Another class of porous particles, arguably called macroporous or cellular particles, contains large voids or cavities and enjoys having wide pores often called windows. Such windows facilitate exchange of matters between different parts of the particles. Open-structured porous particles have found their specific applications. A recent highly regarded application of macroporous particles having interconnected windows is scaffold for tissue engineering.[13,14] Most macroporous microparticles are conventionally synthesised thorough a few physio-chemical techniques including solvent evaporation, polymerization, and seed swelling methods.[15] The formation of pores is usually driven by phase separation occurring during the manufacturing process, which is difficult to finely tune. For example, solvent evaporation method can easily produce porous microparticles, but the diffusion of the internal phase or oil phase during evaporation, which is difficult to control, has dramatic effects on the porosity and window size of the final products. Porous microparticles resulting from droplet polymerization (i.e. suspension) suffer from a low uniformity in both void/window and final particles sizes, whereas seed swelling method, which benefits from a facile generation of uniform nano or micro particles, is limited to microspheres below 10 μm, and to non-uniform

windows.[16] Several attempts have been made to control these properties by varying the formulation, concentration and type of progen, reaction temperature and other triggering conditions within the context of conventional methods.[17,18] However, physio-chemical methods have inherent difficulties in developing void/window of sufficient size and uniformity, and are often limited to small pores.

Cavities or voids can be mechanically housed inside particles by adding a non-solvent, which can be later extracted. The precursors to the production of open-structured macroporous particles are high internal phase double drops. Recently, microfluidic techniques have evolved as an excellent tool for producing uniform double emulsions.[19,20,21,22,23,24,25,26,27,28] When formation of such emulsions is followed by on-the-fly UV polymerization in a microfluidic setup, a wide range of structured porous microparticles can be produced. High internal-phase emulsions in conjunction with microfluidics have been used to produce particles with uniform shapes.[29] The approach has been followed by several research groups to produce porous particles that either internally or externally are uniform.[30,31] However, despite that many reports exist on the fabrication of macroporous particles via microfluidics, window opening has been restricted to off-line methods including UV polymerization and other auxiliary methods. For example, window opening in an offline method occurred by dissolution of the thin film separating the tightly-packed inner cores.[32,33] An off-chip microfluidic photopolymerization approach has also been used to produce anisotropic open polymeric microparticles.[34] Such off-chip methods to create porous microparticles are tedious tasks and do not lend themselves easily to microfluidics. Online lithographic microfluidic polymerization with masking or templating[35,36,37] has been applied onto single-phase fast-curing (acrylate) monomers to fabricate particles with exotic design but the application has not been extended to the continuous creation of windows.

There is a growing evidence that non-spherical particles offer certain advantages over spherical particles. For example, non-spherical particles can be packed more densely than spherical particles.[38] They also benefit from a light weight and behave differently from spherical particles under the same hydrodynamic[39], magnetic [40], and electric conditions.[41] Non-spherical particles can also help to simulate the molecules shape in their self-assembly studies, as most molecules are non-spherical.[42] Non-spherical microparticles are generally difficult to produce due to the domination of surface tension force between two immiscible phases, which resists the formation of non-spherical shapes.[32,43,44,45] Rod-like or cylindrical particles are probably the most common particles second to spherical particles. Porous cylindrical particles are the most important fillers used in fixed beds in chemical engineering applications because of their surface aspect ratios.[46] More importantly, they have been applied in drug-delivery systems for the same reason.[47,48,49,50,51,52,53,54] A microfluidic set up that can produce a wider range of morphologies can be useful in this respect. Drops which are precursor to microparticles, however, can be made to adopt a cylindrical shape when flowing through a confined channel whose diameter is smaller than that of the drop. The technique has been utilised for producing simple rod-like polymeric materials[55] but the application has not been further extended. The nonsphericality of the particles is often imposed by a high inter-phase packing, or the number of inner droplets, or both. In such cases, the shape of particles changes with the number of the inner droplets.[56]

In this report, we demonstrate a two-zone microfluidic generation of cylindrical and spherical/non-spherical drops containing various numbers of internal droplets, followed by their UV polymerization on-the-fly to form open porous microparticles. A porosity hierarchy is often required in porous particles to allow timely and orderly interactions of substrates of different sizes with pores. In this research, however, we only focus on the higher level pores of the hierarchy; voids and windows. Voids are formed when internal water droplets are drained,

and windows when the films separating droplets are ruptured. Typical experiments consisted of producing water/oil/water (w/o/w) double emulsions with controlled number of encapsulated inner droplets, which were then consolidated into porous microparticles through UV photo polymerization. Cylindrical drops were first formed in zone I, where they conformed to the shape imposed by the outer capillary. They then travelled to zone II, where they adopted their most stable morphology. The use of a capillary extension, in zone II, added to the versatility of the approach by allowing cylindrical drops to transform to spherical drops not otherwise achievable under the conditions used for zone I. The critically packed drops for each zone were produced and then polymerised. To produce interconnected windows at relatively low internal phase ratio, the emulsion formulation was manipulated by equalling the inner and outer interfacial tensions. This triggered the collapse of droplets-drop interface during polymerization and exposed the hollow interiors of microparticles. A comparison of close and highly packed drops was made to underline their differences for very first time. The size, shape, and internal structures of particles were manipulated using the flowrates of the phases.

EXPERIMENTAL

Materials

2-ethylhexyl acrylate (EHA, 98.0%, Sigma-Aldrich), isobornyl acrylate (IBOA, 85.0% Sigma-Aldrich), trimethylolpropane triacrylate (TMPTA, 80.0 %, Sigma-Aldrich) were used as monomers. Poly (ethylene glycol)-block-poly (propylene glycol)-block-poly (ethylene glycol) **[**PEG-PPG-PEG, Pluronic L-81, average Mw ~ 2800 g mol^{-1}, and HLB ~ 2] and Irgacure 907 (BASF) were used as surfactant and photoinitiator, respectively, in the middle (monomer) phase. Poly (ethylene glycol)-block-poly (propylene glycol)-block-poly (ethylene glycol) [Pluronic F-127, average Mw ~12,500 g mol^{-1}, and HLB ~ 22] was used as surfactant in the inner and outer aqueous phase.

Microfluidic device fabrication

For the generation of w/o/w emulsions, four micro-capillaries (CM Scientific) were used as the inner (ID: 50 μm, OD: 80 μm), middle (ID: 150 μm, OD: 250 μm), outer (ID: 300 μm, OD: 400 μm) and an extension capillary (ID: 500 μm, OD: 1000 μm), all introduced and aligned symmetrically. The ports were placed on the coupled capillaries, which are resting on the microscope slides, glued (Devcon 5-minute epoxy), and left to harden completely. Capillary surfaces were selectively treated. The capillaries through which oil was flown were made hydrophobic by treatment with n-octadecyltrimethoxysilane while the surface of the capillary where the water went through was made hydrophilic by plasma treatment (Femto Plasma cleaner, Diener).

Procedure

Uniform w/o/w drops were generated by pumping the inner water phase, having 1.0 wt.% of Pluronic F-127 through the middle phase containing 91.0 wt.% of the monomer mixture (composed of 75.0 wt. % EHA, 20.0 wt. % IBOA, and 5.0 wt. % TMPTA based on the total weight of monomer phase), 5.0 wt. % of surfactant Pluronic L-81, and 4.0 wt. % Irgacure 907 photoinitiator dissolved in the monomer phase prior to the experiments. The middle (monomer) phase, engulfing the inner water phase, was then pumped into the external aqueous solution of 1.0 wt. % Pluronic F-127 (outer phase). The syringe containing the monomer was wrapped in an aluminium foil to avoid light penetration.[57] All phases were pumped through the microcapillaries using Harvard pump 11 Elite. The schematic illustration of the 2-zone device used for fabrication of cylindrical and spherical double drops and their polymerization is shown in Figure 1a.

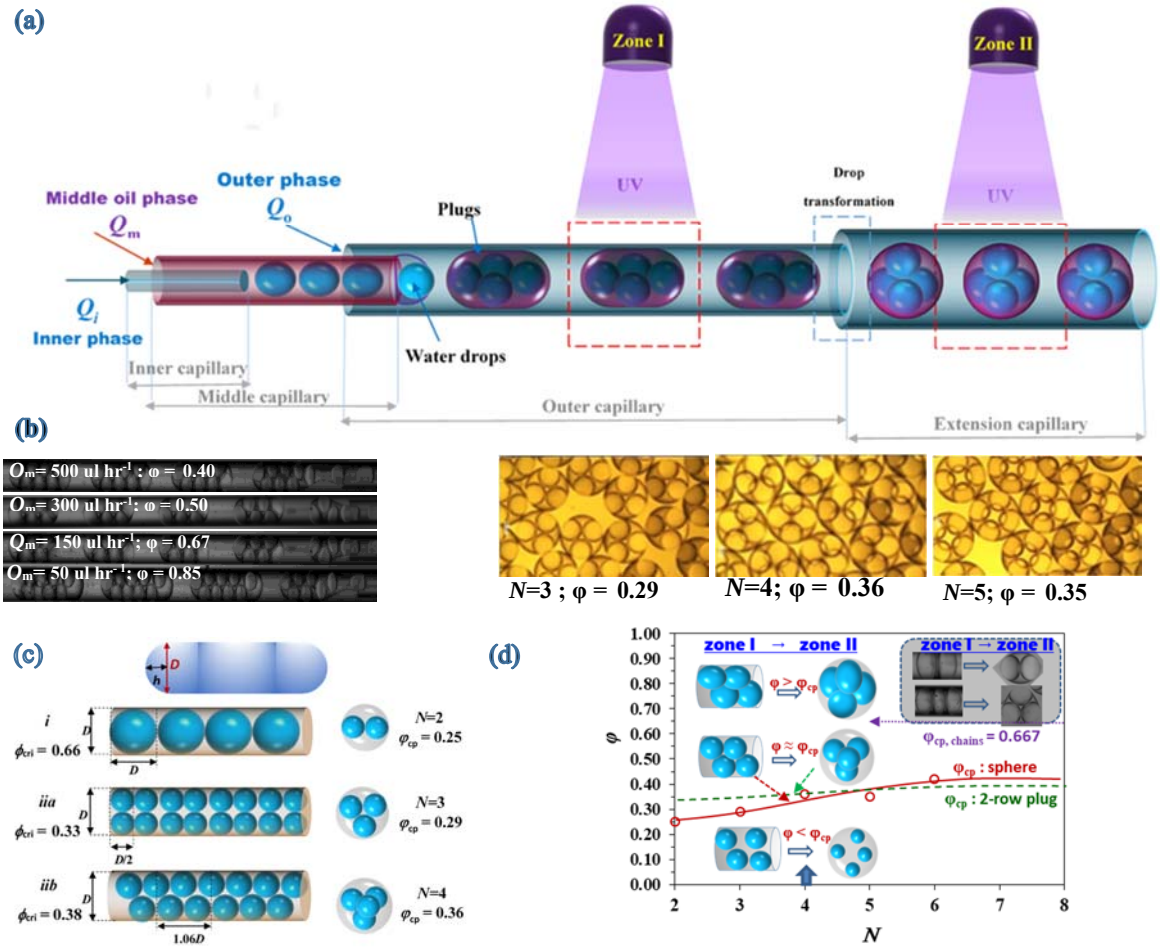

Figure 1. (a) Schematic illustration of the co-flow microfluidic device designed for the preparation of porous microparticles. (b) Typical examples of morphology of plugs and (spherical) drops in zone I and II, respectively, with increasing φ. (c) Illustrations of critically-packed plugs and drops with their corresponding φ_{cp}. The cylinder in the top shows real image of a plug with two caps. (d) The morphology phase map in terms of internal phase ratio (φ) versus the number of inner droplets (N). The line/curves show the locus of critically-packed plugs and spherical drops. In the region above a close packing boundary, respective drops are highly packed, and in the region below the close packing curve, *unconfined region*, drops are not de0nsely packed. The images on the left of dotted boxes show morphology of highly packed plugs in zone I and those on the right show the corresponding morphology in zone II.

RESULTS AND DISCUSSION The generation of drops with various sizes and internal structures was precisely manipulated by varying the flow rates of the inner (Q_i), middle (Q_m), and outer (Q_o) phases. The inner droplets were first formed upstream of the set up in the middle microcapillary. The inner and middle phase joined to form the compound phase at the tip of the middle capillary inside the outer capillary, which was then detached to form compound or

double drops. The compound drops formed in the narrow outer microcapillary, where they were forced to adopt a plug shape, relaxed to gain the spherical shape as they travelled downstream through a wider extention microcapillary (zone II) (Figure 1a). The generated w/o/w plugs or drops were photopolymerized by the UV irradiation (bluepoint 2 easycure, honle, 250 W, 14 mW cm^{-2}) either in zone I or zone II and converted to polymeric microparticles as they passed through the channels. The generation of drops in the microfluidic device was observed by a high-speed video camera (Photron FastCam Ultima APX—monochrome).

Measurements and Characterisation

Plugs and spheres with various structures were observed and sized by an optical microscope (Kyowa Tokyo, Japan, with a camera Moticam 2300 connected to the PC). The morphology, diameter of the windows and droplets (voids), and surface features of the plugs and spheres were assessed by scanning electron microscope (SEM; Hitachi, S4000). For SEM, samples were coated with a thin layer of approximately 5 nm of gold and placed on a stud before analysis. The SEM was operated at 5.0 kV. Viscosities were measured using a scientific rheometer.

Formation of plugs in zone I

We explored the flow conditions under which double drops whose diameter was bigger than the diameter of the outer channel could be produced. Such large drops expanded inside the capillary to form plugs. The diameter of the inner droplets was also controlled to be close to half of the radius of the outer capillary to allow formation of two-row plugs.

The internal phase ratio of drops is defined by:

$$\varphi = \frac{Q_i}{Q_i + Q_m} \quad (1)$$

Figure 1b shows photos for typical variations in the morphology as well as in the number of internal droplets of plugs and spheres, corresponding to zone I and II, respectively, with increasing internal phase ratio φ. Note that the ellipsoidal shape of the internal droplets is an optical artefact emerging from using multiple concentric tubular capillaries.[58]

We define the critical packing phase ratio φ_{cp} as the threshold value of φ at which the core droplets contained in a drop start to contact with each outer and the wall of the drop without being deformed. Any compound drop with a given number of internal droplets N and a phase ratio greater than the corresponding critical packing phase ratio φ_{cp} is called a highly packed drop. Figure 1c shows common configurations exhibited by the internal droplets inside critically-packed plugs, chains, and spheres. For plugs, configuration *i* represents critically-packed single-row plugs, while scheme *iia* and *iib* show configurations for critically-packed two-row plugs.

The critical packing phase ratios for these configurations, defined based on the number of internal droplets N with diameter d enclosed in a cylinder with diameter D and characteristic cell length d or $2d$, are $\varphi_{cp,i} = 0.667$ where $d = D$, $\varphi_{cp,iia} = 0.333$ where $d = \frac{D}{2}$, and $\varphi_{cp,iib} = 0.375$ where $d = 0.53D$ (see supporting information for derivations). The diameter of the internal droplets in the single-row structure *i* is equal to the internal diameter of the outer capillary $d_i = D_{o,ID}$, and the critical packing phase ratio required to achieve this structure is 0.667. Configuration *ii* shows the structure of plugs containing two parallel rows of internal droplets. Droplets in configuration *iia* have diameter d_{iia} which is equal to half of that of the outer capillary; $d_{iia} = D_{o.ID}/2$. The critical packing phase ratio required to achieve arrangement *iia* in plugs is about 0.333. At this phase ratio, the internal droplets are closely contained inside the plug without being deformed. Such a configuration did not form by using a single capillary

set-up for injecting the inner phase. Instead configuration *iib*, which was more stable, was observed for all conditions. The size of internal droplets in configuration *iib* is larger than that in *iia*, and is equal to $d_{iib} = 0.53\ D_{o,ID}$, thus the critical packing phase ratio for this configuration is achieved at $\varphi_{cp,iib} = 0.38$. However, the critical packing phase ratios presented in Figure 1c are only approximates as they underestimate the real values because of the tendency of the plug drops to violate the cylindrical shape, due to their Laplace pressure. The plugs had a cap at each end, as shown in Figure 1c. In theory, one can expect that the volume of the caps changes with the dynamic interfacial tension as well as the size of drops at least for small plugs. In practice, the volume of the caps was found to be almost independent of the size of drops within the range studied. Assuming the volume of the caps can be approximated by a semi ellipsoid with the volume $V_{cap} = \frac{1}{6}\pi D^2 h$ and $h \cong 0.17\ D_{o,ID}$ as defined in Figure 1, and considering that this volume is accessible to internal droplets, there is an error of around 0.04 to φ_{cp} for small plugs (i.e, $N \leq 4$), but the error significantly decreased with increasing *N.* One can expect that the deviation from the simplified cylindrical geometry disappears as the number of internal droplets contained in a plug increases.

Because of further restriction in the space available within spheres, the critical packing arrangement in a sphere containing a given number of internal droplets *N* is achieved at a much lower internal phase ratio than in a cylinder with the same *N* arranged in either one or two rows. Furthermore, the critical packing phase ratio for spherical drops, unlike for cylindrical drops, increases with the number of core droplets. The φ_{cp} for spherical drops with 2, 3, 4, 5 and 6 internal droplets is 0.25, 0.29, 0.36, 0.35 and 0.42, respectively.[56] The illustrative phase map for different morphologies of drops in zone I and II against φ and *N* is shown in Figure 1d. The dotted *green curves* and the continuous *red curve* in the map represent the locus of critically-packed *"cylindrical drops*" and "*spherical drops*", respectively. In the region above a critical packing curve, respective drops are highly packed, and in the region below the close packing

curve, *unconfined region*, drops are not densely packed and thus their internal droplets are relatively small.

The plugs formed in zone I travelled along the flow to zone II, where they adopted a thermodynamically favoured morphology driven by minimisation of interfacial forces. This morphology varied from spherical to semi-spherical, depending on φ and N. Because φ_{cp} at any given N within the range of interest is larger for cylinders than for spheres, critically-packed drops in zone II could only be achieved if their precursors in zone I were highly packed.

Microfluidic production of drops critically packed with droplets of the same size within a wide range of φ, as illustrated in Figure 1d, is a formidable task. This is mainly because a change in the phase ratio φ is practically associated with a change in the size and often the number of internal droplets. The experimental approach to alter φ at constant N was only possible by manipulating the three flowrates simulataneously. By doing so, the compound drops gradually transformed from lean drops in the unconfined region below the critical curve, to "*highly-packed drops"*, crossing the corresponding critically-packed drops curve.

In the "*highly-packed drop*" region, the internal droplets were not spherical anymore, due to their large size and the compression exerted by the external drop, regardless of the zones. Cyclindrical drops with N=2 showed little confomational change from Zone I to II, as shown in Figure 1d. The cylindrical envelope engulfing the inner droplets applies a strong capillary force on the inner droplets, when relaxed in zone II, which leads to drainage of the oil phase from the caps to the film seperating droplets and forms a conical drop similar to the cyclindrical one in zone I. One-row drops containing 3 internal droplets, however underwent extensive conformational change from cyclindrical to triangular as they moved from zone I to zone II. Internal droplets are less vulnerable to defomation than large external drops, as capillary force scales with the reciprocal of drop diamater; $\Delta p = 4\gamma/d$. However, drops with large N could resist the stress applied by the compact inner droplets and remained almost spherical in zone

II, due to the fortunate balance of the outward forces applied by a large number of internal drops on the external drops. There was a threshold in φ above which the outer drops also started to deviate from spherical shape because of increasing stress applied by the deformed inner droplets.

Figure 2a shows a phase morphology map for the plugs in terms of Q_o versus Q_m. For this figure, we used the flow condition $Q_i = Q_m$ corresponding to $\varphi = 0.50$, within the range of 50 µl hr^{-1} - 500 µl h^{-1}.

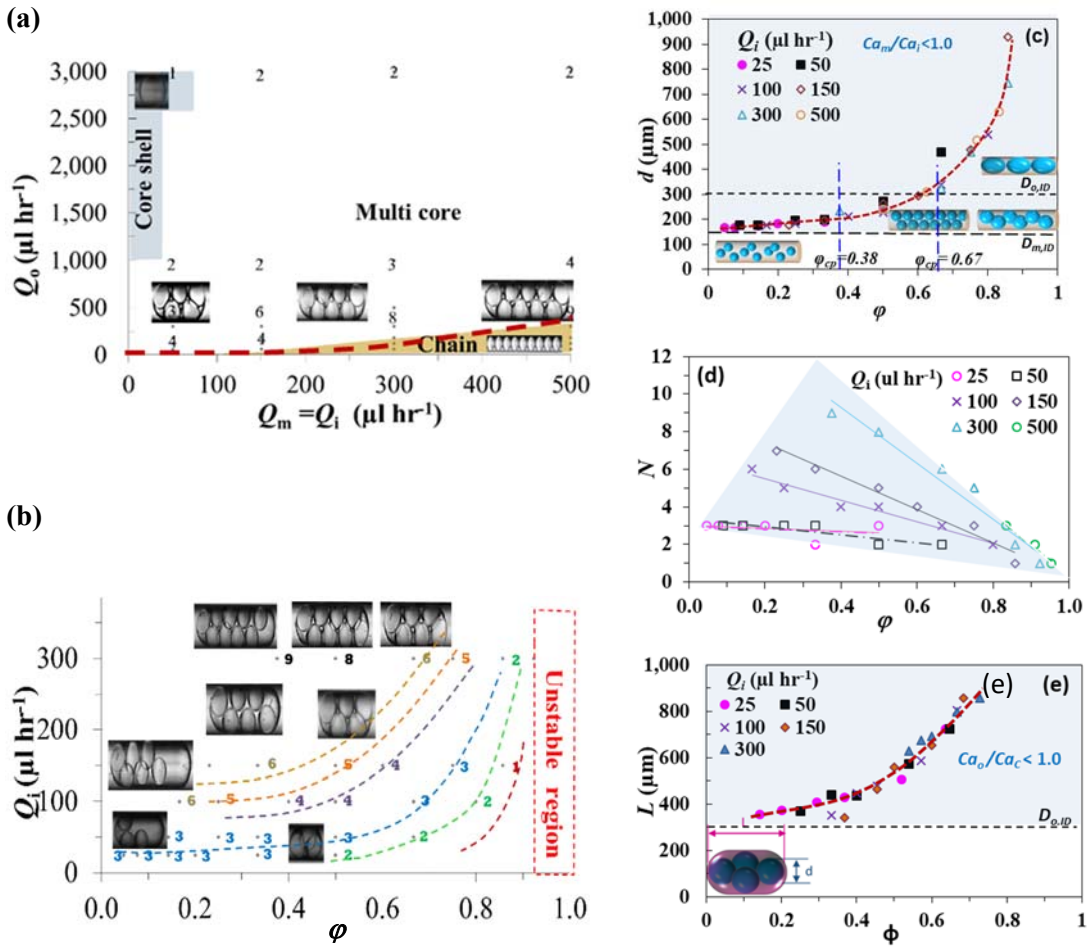

Figure 2. a) A phase map for different domains of plugs in terms of Q_o vs $Q_m = Q_i$. The inset numbers represent the number of internal droplets. **b)** A phase map that shows different domains of plugs in terms of Q_i vs φ and the number of cores N. **c), d)** and **e)** show variations in the diameter of core (d), number of cores (N), and the shell axial length (L), respectively, with increasing φ or ϕ (Q_o=300 µl hr^{-1} for c-e).

At very high Q_o, (> 3000 µl h^{-1}), the middle phase was so frequently ruptured by the outer phase that the inner phase could not be maintained in the middle phase and thus leaked into the

outer phase. In this region the middle phase formed simple oil drops whose diameters were basically smaller than that of the inner water droplets formed in the upstream. Within 1000 µl < $Q_o \leq 3000$ µl h^{-1}, core-shell drops containing one or two inner core droplets started to emerge. The diameter of these compound drops was still smaller than the outer capillary diameter so they adopted a spherical shape. With decreasing Q_o below 1000 µl h^{-1}, gradually larger compound drops with two and more inner droplets were obtained. These drops, expanded along the outer capillary due to their large size and the restrictions imposed by the capillary, forming plugs. It was only at $Q_o \leq 500$ µl h^{-1} that plugs with several internal droplets started to emerge as seen in Figure 2a.

At extremely low Q_o, the shear stress exerted by the outer phase on the compound jet reduced so massively that the jet was not ruptured at a short length anymore. This allowed the jet to widen in the capillary (i.e, jet widening) forming continuous chains.[23] The dashed line in Figure 2a marks the domain of the chains. The data points in the region above the dashed line refer to two-row plugs, and below the dashed line refer to chains, where a continuous jet of the middle phase containing many internal core droplets was formed. The range of Q_o within which transition from plugs to chains occurred was narrow, however, it increased significantly with increasing Q_i.

The drop size in a typical capillary co-flow system is determined by a competition between interfacial tension and hydrodynamic forces. The formation of drops is often discussed in terms of capillary number *Ca*, which represents the relative importance of disruptive viscous forces acting on fluid's interface compared to its cohesive interfacial force

$$Ca_j = \frac{\mu_j v_j}{\gamma_{jk}} \qquad (2)$$

where μ is the viscosity, v is velocity at the point of drop rupturing and γ is the interfacial

tension. The indices *j* and *k* refer to different neighbouring phases, which can be *i* for the inner phase, *m* for the middle phase and *o* for the outer phase.

Inner droplets were formed in the 1st stage. During the 2nd stage, the middle oil phase containing the inner water droplets, or the compound phase indicated by index *c*, was ruptured to plugs. Considering the common interfacial boundary between the compound phase and the outer phase, the capillary ratio of these two phases scales with $\frac{Ca_o}{Ca_c} = \frac{\mu_o v_o}{\mu_c v_c}$. The viscosities of the inner and outer water phase containing the hydrophilic surfactant and the middle phase containing the lipophilic surfactant was 1.7 cp and 1.4 cp, respectively. The average velocity of the compound phase (inner water phase + middle oil phase) and the outer (water) phase are related to the flow rates of these phases and the capillary cross sectional areas (see supporting materials). For our capillary arrangements, the relation between A_m and A_o was found to be $A_m \cong 0.60A_o$, so $\frac{v_o}{v_c} = \frac{A_m Q_o}{A_o(Q_i+Q_m)} = \frac{0.6Q_o}{(Q_i+Q_m)}$. The red dotted-curve indicated on Figure 2a defines the experimentally found transition between plugs and chains. The curve is an exponential one but for the sake of simplicity we approximate it by a linear correlation $Q_o \cong {}^1/_2\, Q_i$. Assuming that the compound phase has a viscosity similar to that of either oil or water phase so $\mu_o/\mu_c \approx 1.0$, and applying $Q_i = Q_m$ a nd $Q_o \cong {}^1/_2\, Q_i$ for the conditions of Figure 2a, then one can find that transition line is represented by $\frac{Ca_o}{Ca_c} = 0.15$. To rupture the compound phase by shear stress exerted by the outer phase, the capillary ratio should be greater than one; Ca_o / Ca_c >1. The ratio suggests that the widening jet conditions are dominant at the boundary. This ratio is consistent with the values reported by Nabavi et al. for the widening jet conditions that allowed chain of droplets to form in a single-stage flow-focussed method.[23]

Figure 2b shows a morphology map for the resulting plugs in terms of Q_i and internal phase ratio φ. To construct this figure, we fixed the flowrate of the outer phase at Q_o = 300 µl hr^{-1} and altered Q_i and Q_m within 25-500 µl hr^{-1} in a systematic way to change the internal phase ratio.

The number of internal droplets contained in the plugs is also shown on the map. At low values of φ (i.e., low Q_i/Q_m) plugs were not highly packed by droplets, as expected. Such plugs are not of any use for making open structures, but are useful for fabricating closed structures. Highly packed drops started to emerge at $\varphi \sim 0.35$. One can see from this figure that the domain of plugs with a given number of internal droplets changed almost exponentially with increasing φ. This indicates that highly packed plugs with a given number of internal droplets could be only produced at extremely high flowrates of the inner and middle phases (i.e, high Q_i and Q_m).

It can also be inferred from this map (Figure 2b) that at a given Q_i, the increase in the internal phase ratio φ was associated with a decrease in the number of internal droplets until eventually plugs with one internal droplet, capsules, were obtained at an extremely high φ. At a given φ, the number of internal droplets could be increased by a simultaneous and proportionate increase in Q_i and Q_m.

Figure 2c shows an interesting pattern in which the size of internal droplets, d, increased consistently with increasing φ for different sets of flow conditions, regardless of the absolute values of the flow rates. In the two-stage method used here, the inner droplets were first formed in the upstream, in the middle capillary, and then housed inside the oil drops forming the compound phase. The inner and middle phases shared the same interface, so their capillary ratio is

$$\frac{Ca_m}{Ca_i} = \frac{\mu_m v_m}{\mu_i v_i} \qquad (3)$$

See supporting materials for the way velocities have been calculated. Combining eqs (1-3) and noting that $Q_i = A_i v_i$ and $Q_m = A_m v_m$, the following equation can be derived that relates Capillary ratios to φ:

$$\frac{Ca_m}{Ca_i} = \frac{\mu_m A_i}{\mu_i A_m}\left(\frac{1}{\varphi} - 1\right) \qquad (4)$$

Equation (4) suggests that for a given microfluidic setup, the shear stress applied on the inner phase only depends on the relative flow rates (i.e., φ) and not on their magnitudes. In other words, using a high Q_m, at a given Q_i, increases the shear stress applied on the inner phase. The size of internal droplets increased with increasing φ, due to the associated decrease in the shear stress. Calculations show that the relation $\frac{Ca_m}{Ca_i} < 1.0$ was dominant for most conditions used in this research, except for low values of φ (~0.05).

By the same token, it can be shown that the capillary ratio smaller than one was accompanied by the ratio of Weber number of the inner phase (defined as the ratio of inertial forces over the interfacial forces) over the capillary number of the middle phase being larger than one for all conditions except for low values of φ;

$$\frac{We_i}{Ca_m} = \frac{(\rho_i v_i^2 D_{i,ID})/\sigma_{co}}{\mu_m v_m/\sigma_{im}} = \frac{\rho_c v_c^2 D_{i,ID}}{\mu_o v_o} > 1.0 \qquad (5)$$

where $D_{i,ID}$ is the internal diameter of the inner capillary where the internal phase was pumped through. This confirms that the inertial forces were dominant.

There was a steep increase in d at higher φ, a trend clearly observed in Figure 2c. The internal droplet diameter at $\varphi \approx 0.65$ was 300 μm, which is equal to the internal diameter of the outer capillary. This is the point at which one-row plugs with diameter of the internal drops being equal to the inner diameter of the outer capillary $D_{o,ID}$ formed. Beyond this threshold, internal droplets became larger than $D_{o,ID}$ and then stretched along the capillary. Figure 2c was produced using $Q_o = 300$ μl hr^{-1}. Using a lower Q_o, would allow plugs with larger N to develop. At extremely low Q_o, chain of droplets formed as explained before. We note that the size of the internal droplets was independent of the outer phase flow rate Q_o because of the two-stage protocol used.

The discussion above is illustrated in Figure 2d that shows the increase in d with increasing φ was associated with a decrease in the number of internal droplets (N). At low to intermediate φ, plugs with several internal droplets were formed. At φ = 70%, plugs could contain only up to 4 internal droplets, depending on Q_i. The largest N was obtained at the lowest Q_i used. At φ = 80%, plugs with upto 3 internal droplets in a row could be formed. Further increase in φ led to formation of plugs with two internal droplets in a straight one-row structure. Eventually, with further increase in φ above 85%, plugs with one internal core droplet, or plug capsules, emerged. This is due to the formation of a stable biphasic jet at high inner phase flowrate inside the middle capillary, which emulsified at the tip into core-shell drops with an ultrathin shell. [59]

The combined effect of the number and size of internal droplet reflects on the length of the plugs, which is an important physical property of plugs. We note that the diameter of the plugs was equal to the internal diameter of the outer capillary. Figure 2e shows variations in the length of the plugs L with ϕ for different values of Q_i at a constant Q_o. ϕ is the phase ratio of the compound phase in the final emulsion defined by

$$\phi = \frac{Q_i + Q_m}{Q_i + Q_m + Q_o} \qquad (6)$$

It is useful to show the results in terms of ϕ rather than φ because the former scales with the shear stress applied on the compound phase: $\frac{Ca_o}{Ca_c} = \frac{\mu_o A_c}{\mu_c A_o}\left(\frac{1}{\phi} - 1\right)$. The experimental conditions related Figure 2e can be best described by $\frac{Ca_o}{Ca_c} < 1.0$, indicating that the jet widening mechanism, due to the high inertial forces of the compound phase, was operative. Long plugs were formed at high ϕ. The length of the plugs reduced with decreasing ϕ (i.e, decreasing Q_m at a given Q_i) until a plateau length close to the inner diameter of the outer capillary ($D_{o,ID}$) was reached. One should note that ϕ increases with decreasing φ at a constant Q_o.

From Figure 1 one can infer that the length of closely packed two-row plugs can be related to the diameter of individual droplets and their number by (N/2)×d, in particular if N is even. If this term is plotted against φ and compared with the experimental L (not shown), one can find that initially the experimental L is much larger than (N/2)×d, because the plugs were not completely packed with internal drops. But as φ approached the close packing ratio, the two values converged.

Transformation of drops in zone II

As soon as plugs entered zone II, they transformed to the most thermodynamically stable arrangement.[56] The re-arrangement was completely repeatable and always occurred in a same way. The resulting compound drops formed by the transformation of plugs in zone II are shown in a next section along with their corresponding microparticles to save space. Assuming that the plugs transformed in zone II are spherical, their diameter can be related to the dimensions of their precursors in zone I using equation $D_s = \left(\frac{3}{2} L D_{o,ID}^2\right)^{1/3}$, where D_s is the equivalent spherical diameter of plugs in zone II. The predicted values of D_s for highly-packed plugs ($\varphi > \varphi_{cp}$) that entered zone II were still close to the measured values within an intermediate range of φ, despite the internal phase ratios being greater than that of the close packing. The shape of the (outer) drops, however, was distorted at high φ, because of the stress applied by the compact inner phase. The morphology of drops in zone II varied from spherical (S) to semi-spherical (SS) with increasing φ above φ_{cp} at a given N, but reversely from semispherical to spherical with increasing N at a given φ, unlike cylindrical plugs in zone I whose shape was almost independent of φ and N due to the geometrical restriction imposed by the capillary. Overall, drops with different morphologies could be produced, however, there existed only one morphology that could fit a given N and φ in any polymerization zones.

Formation of windows during UV polymerization

The formation of windows during polymerization depends on the interfacial and bulk properties of the monomer and water phases used, in addition to their phase ratio. Windows are formed during polymerization mainly due to the stress resulting from shrinkage; that is the density difference between the monomer and polymer gel phases.[60] A droplet moving in a microchannel will only have a small fraction of a second to polymerise by the UV light and therefore should be highly reactive. Furthermore, it should undergo a high degree of shrinkage during polymerization. To allow windows to emerge, in particular at low φ, a careful selection of monomers is therefore essential. We investigated a number of monomers and selected a set of acrylic monomers that are highly reactive with a considerable shrinkage (see supporting information). Interestingly such polymerization formulations that do not allow window openings may find applications for encapsulations where closed structures are often required.

Ideally, the film separating the inner core droplets and the outer shell drop should be made to rupture during polymerization, allowing the internal water to escape the particle leaving open windows. However, when the double drop templates (that contained no surfactant in the inner water phase) were exposed to UV, the resulting microparticles showed no sign of opening, as seen in Figure 3a. In a similar study, highly packed double drops produced via microfluidics did not open up when they underwent UV polymerization.[56] Off-chip methods such as the use of solvent have been often used to fabricate open structures by dissolving the thin films.[32,33]

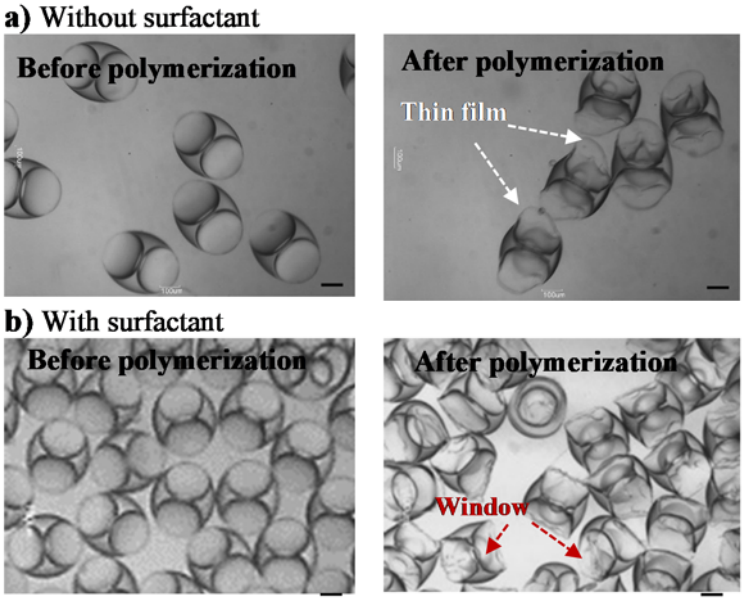

Figure 3. Optical micrographs images of uniform double drops and resulting polymer particles with 2 internal core droplets, **a)** without surfactant in the core phase showing no window, and **b**) with 1% water-soluble surfactant (Pluronic F-127) in the core phase showing windows. Scale bar is 100 μm.

The production of highly porous materials by polymerization of high-internal phase emulsions is a routine in chemical industries.[4,8] The close packing ratio of 0.74 is the minimum requirement for making open structures using uniform droplets, though for polydisperse emulsions the ratio should be much higher. In practice, internal phase ratios in the region of 0.80-0.90 are often used.[4,14,30] Under such conditions, the films seperating drops are very thin and can be easily ruptured to form porous structures during polymerization, due to the stress resulting from the the polymer shrinkage. Double drops containing a few internal droplets have a much lower close packing phase ratio threshold than emulsions in unconfined space, due to geometrical restrictions imposed by the confinement, which is usullay within a range of 0.25-0.40. For that reason the films seperating the inner droplets are neither thin along the surface, nor uniform, demonstrating the challenges involved in fabricating open structures in confined spaces. There are a few ways to enhance droplet escape during polymerization. One way is by adding an electrolite to the inner phase that induces an inflow of water from the outer

continuous phase to the inner water phase and swells the inner phase, due to the osmosis effect, which may lead to escape. This was attempted, but abondoned because of the undesired extensive change in the internal phase ratio. The other approach is to impart kinetic instability to double drops. According to the Bancroft‘s rule, the phase in which a surfactant is more soluble tends to become the continuous phase.[61] In our primary formulation, the outer phase contained 1.0 wt% water-soluble surfactant Pluronic F-127 and the middle oil phase contained 5.0 wt% oil-soluble surfactant Pluronic L-81 in the stable w/o/w emulsions made. The presence of surfactant in the oil phase was required to stabilise the inner water droplets. In the modified formulation, we used the same water phase containing 1.0 wt.% surfactant for both the inner and outer phases, against the backdrop of increased instability of double drops, so that $\gamma_{mo} \approx \gamma_{im}$. Figure 3b clearly shows this policy enhanced the tendency of the inner drops to join the outer continuous phase during polymerization, via escaping the middle phase, and led to the opening of the windows. Adoption of such a methodology in conventional mechanical production of high internal phase emulsions is not possible due to premature escape of inner droplets caused by extensive deformation of drops during stirring. In contrast, the double drops formed in the microfluidic setup with the inner phase containing the surfactant remained stable during their journey in the capilary as long as they were not subjected to a significant shear. A similar concept, though in different context, has been previously used to transform a high-viscosity jet, which was difficult to rupture, to unstable core-shell drops which produced uniform drops after the escape of inner cores.[62] The concept was also used to help bubbles escape air-filled alginate microfiber, thus producing a wide range of anisotropic particles.[63] The methodology described above created particles with external and internal interconnected windows using unassisted rupturing. The methodology also suggests a practical way to switch from open structures to closed structures such as capsules by using a small alteration in the formulation at the same process conditions.

Microparticles formed in Zone I

The compound drops were polymerized on-the-fly as they passed through the UV zone I. Critically packed plugs did show little sign of opening, due to highly asymmetric nature of the monomer films separating the internal droplets. We therefore conducted the polymerization for plugs at $\varphi = 0.50 > \varphi_{cp}$ ($Q_i = Q_m = 150$ µl hr^{-1}). The top insets in Figure 4a-d show the formation of the precursor liquid plugs inside the capillary and the top right insets show the optical micrographs of their corresponding polymeric plugs, while the SEM images of the resulting plugs are the main focus of this figure. The conditions used to produce these highly-packed plugs are outlined in the caption of Figure 4.

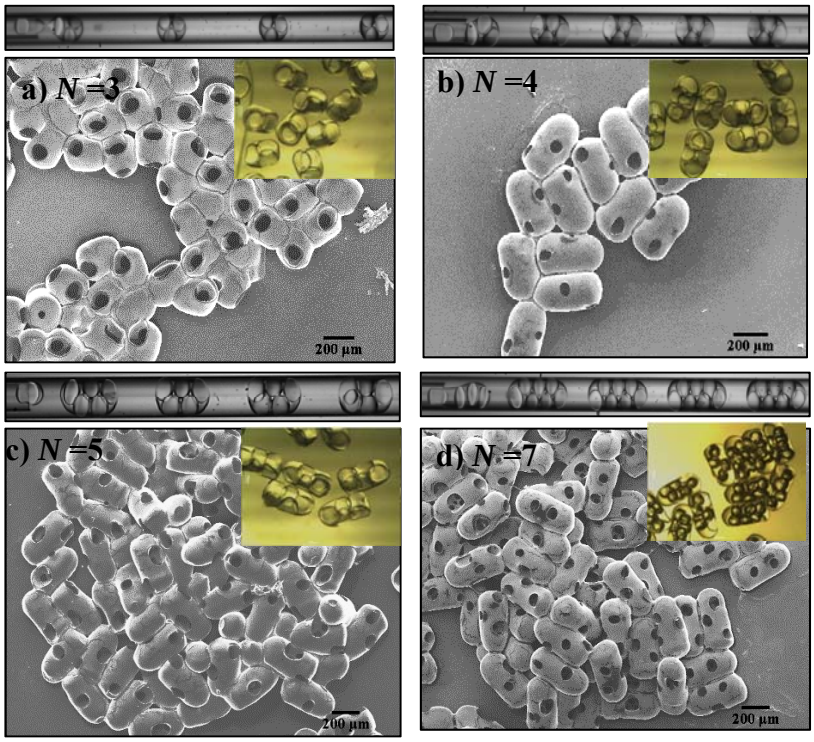

Figure 4. Images showing the formation of plugs (top inset) and SEM images of the corresponding microparticles obtained at fixed $Q_i = Q_m$=150 µl hr^{-1} for **a)** triple cores formed at Q_o=500 µl hr^{-1}; **b)** quartet cores formed at Q_o=400 µl hr^{-1}, **c)** quintet cores formed at Q_o=300 µl hr^{-1}; **d)** septet cores formed at Q_o=200 µl hr^{-1}. The top right insets show microscopic images of the plug-like microparticles, with different numbers of cores. The scale bar is 200 µm.

One can see from Figure 4a-d that the number of external windows on the surface of the microparticles is equal to the number of internal droplets *N*. That means there was a maximum

of one external window per internal droplet. This is understandable as drops were aligned in two rows, with the thickness of the shell being much greater on one side of the internal droplet than on the other side. Film rupture only occurred across the thinnest shell.

One-row plugs were formed at higher internal phase ratios, as explained before. A high φ (>0.667) depressed the shear stress acting on the inner phase and formed large internal droplets that assembled in a single row. Examples of high internal phase (one row) plugs with one, two and three internal droplets are shown in Figure 5. Plugs with a single core (see Figure 5a) were basically capsules with no interconnecting window, due to their symmetric structure. Capsules with closed structure will find application in controlled release and drug delivery where a large surface area per unit volume is required.[51,52,53]

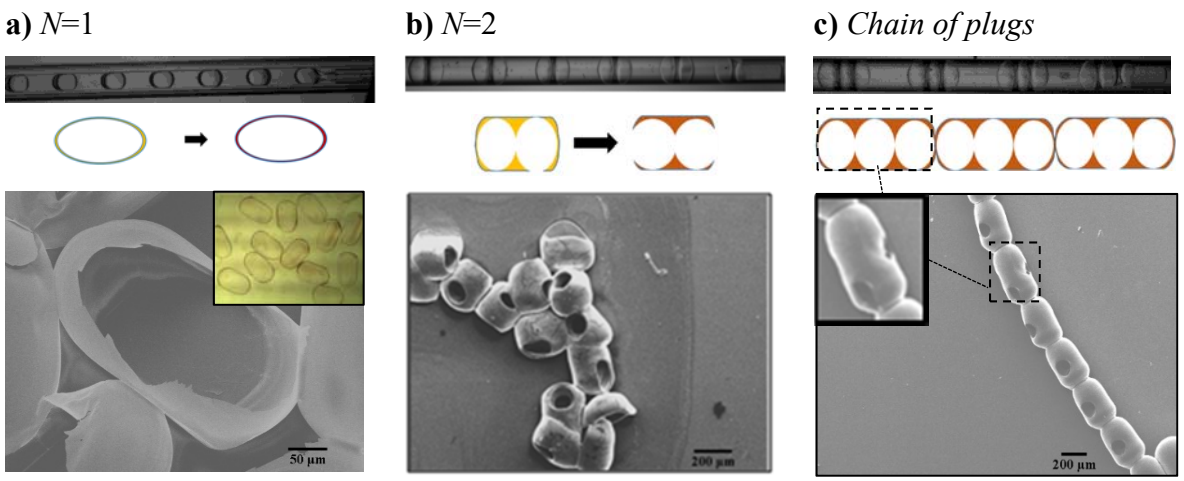

Figure 5. SEM images of the plugs obtained with **a)** $N = 1$ (Q_i=1000 µl hr^{-1}, Q_m=100 µl, and $\varphi = 0.90$); **b)** $N = 2$ (Q_i=300 µl hr^{-1}, Q_m=50 µl hr^{-1}, and $\varphi = 0.85$); and **c)** *N=3* (Q_i=500 µl hr^{-1}, Q_m=100 µl hr^{-1}, and $\varphi = 0.83$). Also (c) shows a chain of porous plugs with three cores fused together. For all conditions: Q_o =300 µl hr^{-1}.

Plugs with two internal droplets (Figure 5b) were similar to cylinders containing two cavities with conic poles connected via an internal window. One-row plugs with more than three internal cores did not have consistent structures probably due to a large interfacial area developed between the inner and outer phase, separated by a thin film of the middle monomer

phase, and non-uniform UV radiation across the length of plugs. An example is shown in the inset in Figure 5c for plugs with 3 internal droplets.

We were not able to fabricate chains with a large number of internal droplets as they did not polymerise on-the-fly. These chains were stuck in the capillary as soon as they were exposed to the UV. The possible outcome from such a study remains to be evaluated in the future, due to inconsistent openings that one-row plugs demonstrated. It has been shown before that chains can easily be polymerised if the polymerization reaction occurs uniformly outside the capillary in a buoyancy driven system.[64] One could expect a highly packed single chain of droplets to undergo multiple film ruptures across its length and break up into a range of uniform particles such as frustums and ⧫ particles, when exposed to uniform UV radiation.[63] However, we managed to produce porous chains consisting of a number of short plugs in two steps, as shown in Figure 5c. In the first step short plugs were produced in the upstream and then forced to fuse together in the downstream of the microfluidic set up to form a chain. The short plugs used as the repeating unit in the chain contained 3 internal droplets, but could be any plug.

Microparticles formed in Zone II

The use of an extension capillary had two advantages. Firstly, it reduced the velocity of drops by 1/3, tripled the exposure time of the drops to the UV, and thus assisted rapid polymerization. Secondly, it allowed drops to be produced in a smaller outer capillary, which had three times larger capillary number than the extensional capillary, and then transported in the extensional capillary, where a high *Ca* number was not required anymore. This implies a significant reduction in the required Q_o for obtaining drops of a given size. Cylindrical drops formed in zone I were allowed to pass through this zone unpolymerized, and enter zone II, where they relaxed and conformed to their most stable morphology before being polymerised.

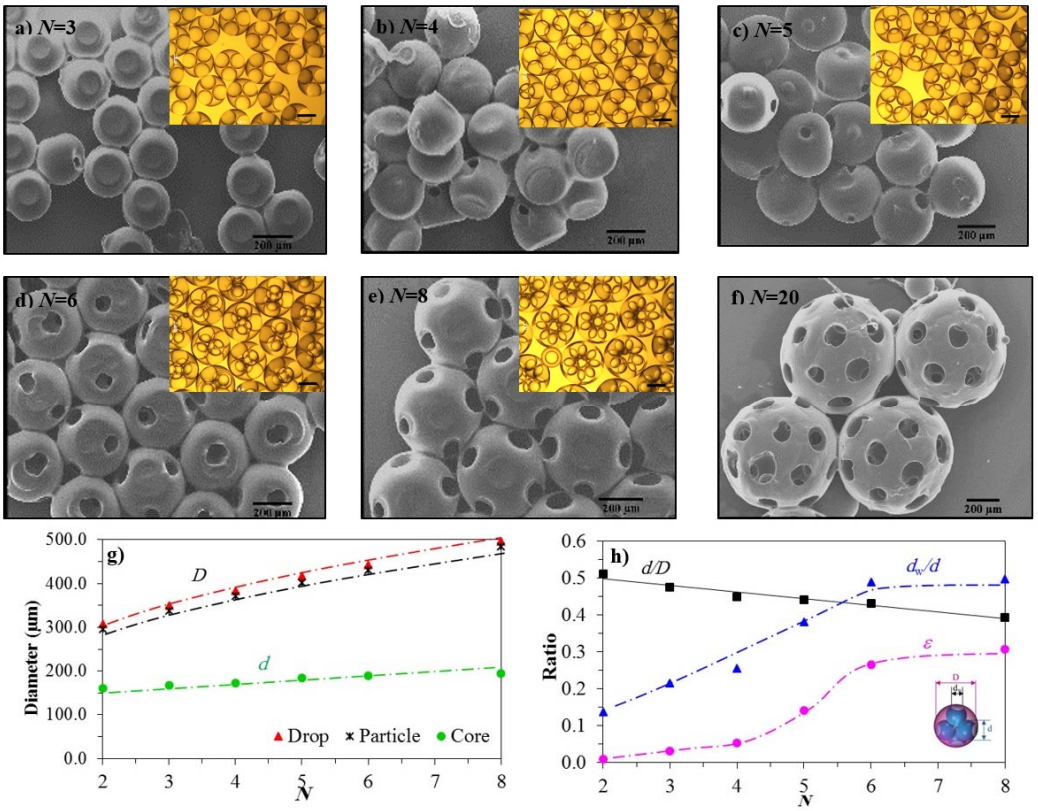

Figure 6. SEM images of porous microparticles produced using closely-packed precursor drops, with a given number of core droplets (N) obtained at fixed Q_i =200 µl hr^{-1} ; **a)** N = 3 (Q_m =450 µl hr^{-1}, Q_o = 2000 µl hr^{-1}; φ = 0.31); **b)** N = 4 (Q_m =350 µl hr^{-1}, Q_o = 1000 µl hr^{-1}; φ = 0.36); **c)** N = 5 (Q_m =350 µl hr^{-1}, Q_o = 700 µl hr^{-1}; φ = 0.36); **d)** N = 6 (Q_m = 270 µl hr^{-1}, Q_o = 400 ul hr^{-1}; φ = 0.42); **e)** N = 8 (Q_m =270 µl hr^{-1}, Q_o = 300 µl hr^{-1}; φ = 0.43); **f)** N = 20 (Q_m = 270 µl hr^{-1}, Q_o = 100 µl hr^{-1}; φ = 0.42). Insets show optical micrograph images of the corresponding critically-packed drops. The scale bar is 200 µm. **g)** Diameter of the internal core (d_w), external drop (D) and final particle versus the number of cores N; **h)** relative size of internal droplets to the external drop *(d/D)*, relative size of windows on the surface of microparticles d_w with regard to the diameter of the core d_w/d, as well as the relative magnitude of opening area on the surface of a microparticle ε versus the number of cores N.

Microparticles produced by polymerization of critically-packed drops*:* Figure 6a-f shows micrograph images of the generated critically-packed drops with a given N (inset) and their polymerised products. SEM images in Figure 6a-f reveal an interesting feature of the critically-packed polymeric drops. Drops containing two internal core droplets did not open up at all, but those with 3-5 internal droplets showed increasingly occasional opening, as seen in Figure 6a-c. However, critically-packed microparticles with $N \geq 6$ showed complete window opening (as seen in Figure 6d-f). Figure 6F, in particular, shows the interconnected structure of the windows.

Drawing the attention back to the effects of the number of internal droplets N on the size of drops, one could see from Figure 6g that the size of the external drops increased with the number of the internal cores. The size of the internal droplets also showed a small change with N, due to the associated increase in φ (see Figure 2c). The shrinkage scales with the volume fraction of the monomer phase, 1- φ, which was not greatly different for N = 2-6. On average, the diameter of the polymeric microparticles was smaller than the original drop size by around 5.0 % for all cases. This also shows that unlike conventional polyHIPEs that do not shrink externally during polymerization, due to the presence of non-compressible water droplets, and windows only open up during post-polymerization, the open porous structures formed on the fly do shrink.

For double drops with a low internal phase ratio and spatially-varying shell thickness, the thinnest part of the shell is the weakest, and most vulnerable point to rupture. These weak points locate where the internal droplets touch the shell drop. It has been reported that similar points across multiple-core polymer shell capsules buckled in response to a high external capillary pressure.[65] The number of external windows on the surface of the microparticles was found to be equivalent to the number of internal droplets for $N \geq 6$. The relative size of the internal droplet with respect to the size of the outer drops (d/D) decreased with increasing N but both the relative diameter of the windows with respect to the diameter of internal droplets, d/d_w, and the relative opening area on the surface of microparticles, $\varepsilon = Nd_w^2/D^2$, increased as seen in Figure 6h. The methodology can be extended to drops containing a large number of inner droplets, as seen in Figure 6f for particles with N = 20. The d_w/d for the particles with N = 20, however, was 0.27, indicating that there is a maximum in d_w/d achievable within N = 8-20. However, ε always increased with increasing N due to the associated, and inevitable, increase in φ.

Microparticles produced by polymerization of highly-packed drops: A series of experiments was conducted with the phase ratio of the inner phase being maintained constant at $\varphi = 0.71$. Because the close-packing state was exceeded, $\varphi > \varphi_{cp}$, the core droplets confined in the shell drop re-arranged themselves into a distinct configuration due to their capillary pressure as well as that of the outer drop. This configuration depended on the number and size of core droplets, but was reproducible. Such a high φ was employed to achieve a small shell thickness across neighbouring droplets, enhance film rupturing, and create larger relative opening areas. The alteration in N at the constant $\varphi = 0.71$ was brought about by gradually decreasing Q_o. Starting with highly-packed elipsoidal drops containing two internal core droplets (N=2), whose φ_{cp} is 0.25, we gradually transformed these drops to highly-packed drops with more inner droplets at the same φ. The SEM images of the resulting porous microparticles, Figure 7af, show particles have as many internal droplets as external windows. The conditions required to obtain these highly-packed drops are outlined in the caption of Figure 7.

By comparison, the highly packed drops opened up more consistently for all N than the critically packed ones due to a higher φ used and as a result a significant stress applied on their over-stretched thin interfaces during polymerization (i.e. shrinking), as expecetd. Symmetric morphologies such as simple core-shell drops (see Figure 7a for N=1) did not open due the balanced forces applied on the uniform shell, regardless of φ.

From Figure 7g shows variations in the diameter of drops with N. The use of the two-stage microfluidic setup allowed to maintain a precise control over the size of the inner cores at constant φ. The double drops increased in size as they accomodated more inner droplets.

The relative size of the windows with regard to the size of the cores, d_w/d, and relative surface area of interconnected windows with regard to the external surface of particles, ε, decreased with increasing N, as shown in Figure 7h. This is an interesting feature of highly packed drops that increasing their N at constant φ adversely affected their relative opening area ε and window

diameter d_w/d. However, critically-packed drops showed an increase in d_w/d and ε with increasing N, but that was partly due to the associated increase in φ, and to the fact that drops with $N<6$ openned up occasionally.

An sphericity factor was used to measure how closely the shape of the highly packed drops approached that of a mathematically perfect sphere. One can see from the SEM images in Figure 7a-e and the measured spherisity factor f defined in Figure 7i that the violation of sphericity was significant for $N = 2$, but gradually decreased with increasing N. Compound drops with a large number of internal droplets resisted deformation due to balanced multiple capillary forces exerted by many inner droplets. Overall, the external drops in zone II changed shape from ellipsoid to semispherical with increasing N at constant φ.

In order to examine the mechanism of window formation and explore the effects of polymerization conditions on the particle morphology development, we monitored the time evolution of morphology of a highly-packed drop with $\varphi = 0.71$ containing 2 internal cores, $\varphi > \varphi_{cp} = 0.25$. The polymerization was conducted thermally and monitored using an optical microscope. Figure 7j shows that particles did not open under slow polymerization conditions, but their spherisity factor f further increased during polymerization. This suggests that a rapid polymerization not only served to open up windows at low φ, but also freezed the morphology of drops and assisted particles with a simillar morphology as their precurser drops to emerge.

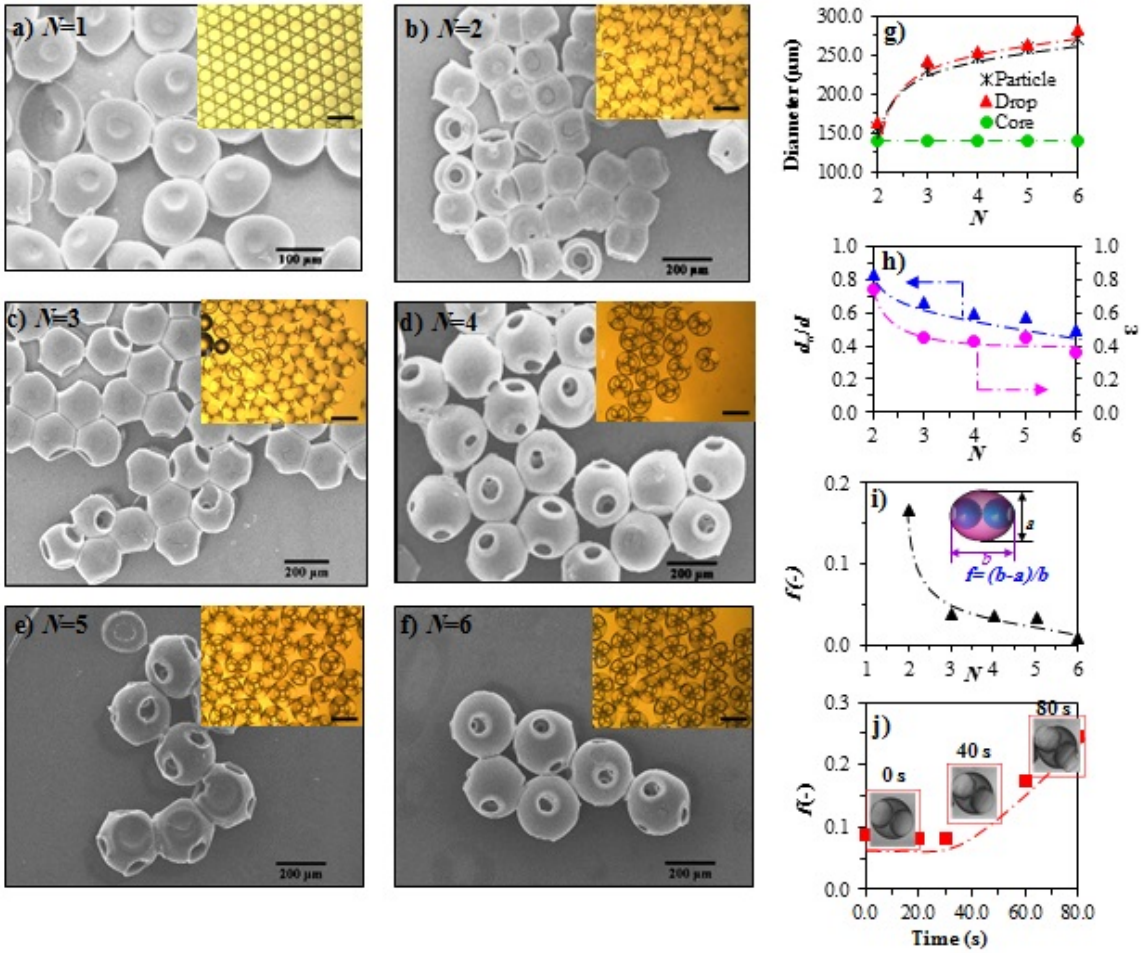

Figure 7. SEM images of the highly packed drops (insets) and microparticles with φ = 0.71[Q_i =500 µl hr^{-1} and Q_m =200 µl hr^{-1}]. **a)** N = 1 (Q_o= 5000 µl hr^{-1}) **; b)** N = 2 (Q_o= 3000 µl hr^{-1})**; c)** N = 3 (Q_o= 5000 µl hr^{-1})**; d)** N = 4 (Q_o= 1000 µl hr^{-1})**; e)** N = 5 (Q_o= 800 µl hr^{-1})**; f)** N = 6 (Q_o= 600 µl hr^{-1}). Insets show optical micrographs of the corresponding highly-packed drops. The scale bar is 200 µm. **g)** Diameter of the external drops**,** internal droplets and particles versus number of cores N; **h)** The relative diameter of the window d_w/d, as well as the relative magnitude of opening area ε versus N; **i)** The sphericity (f) of the external drop versus N; **j)** Time-dependent change in the sphericity (f) of a drop containing two core droplets during thermal polymerization.

One can realise that using a high internal phase ratio for fabricating porous particles is advantageous as it renders a high porosity and an opened structure to the particles. When such a high internal phase ratio drops are made, however, there might be a conflict between the desired morphology and the one dictated by the internal phase ratio. Cylindrical porous particles whose shape is independent of their φ and N can provide an answer to such dilema.

1. CONCLUSION

Uniform w/o/w emulsions, produced via glass-capillary based microfluidic technique, were used as precursors to fabricate various porous microparticles via UV polymerization. The size, porosity and morphology of the resulting microparticles were controlled by the flow rate of individual phases and the packing structure of the inner droplets, as well as by the restriction imposed by the external geometry. Polymerising the drops led to the rupturing of the thin walls of the droplet-drop, exposing the hollow interiors of microparticles. Windows consistently formed during polymerization for highly packed plugs and drops, due to a significant stress applied on the over-stretched asymmetric interfaces during shrinkage. While the internal phase ratio of drops affected the porosity of particles, it hardly affected the cylindrical shape of the microparticles. Critically-packed spherical drops, whose morphology development during polymerization was investigated for the first time, only opened up if they had more than 6 internal droplets. The fabrication of porous microparticles, with tunable window sizes and structures can open new vistas for many potential applications.

Supporting Information: The supporting information contains relations between velocity and flow rates, the diameter of spherical droplets in critically packed plugs, the critical packing phase ratio for different configurations, and the optimisation of formulation.

Table of Contents Graphic

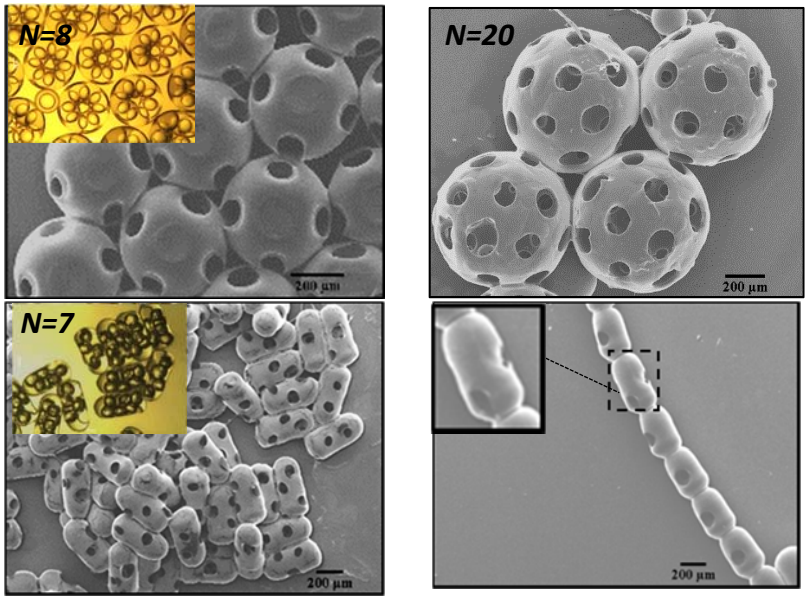

References

(1) San Manley, S.; Graeber, N.; Grof, Z.; Menner, A.; Hewitt, G. F.; Stepanek, F.; Bismarck, A. New insights into the relationship between internal phase level of emulsion templates and gas–liquid permeability of interconnected macroporous polymers. *Soft Matter* **2009**, *5*, 4780-4787.

(2) Jiang, J. X.; Trewin, A.; Su, F.; Wood, C. D.; Niu, H.; Jones, J. T.; Khimyak, Y. Z.; Cooper, A. I. Microporous poly (tri (4-ethynylphenyl) amine) networks: synthesis, properties, and atomistic simulation. *Macromolecules* **2008**, *42*, 2658-2666.

(3) Ben, T.; Ren, H.; Ma, S.; Cao, D.; Lan, J.; Jing, X.; Wang, W.; Xu, J.; Deng, F.; Simmons, J. M.; Qiu, S. Targeted synthesis of a porous aromatic framework with high stability and exceptionally high surface area. *Angewandte Chemie* **2009**, *121*, 9621-9624.

(4) Okay, O. Macroporous Copolymer Networks. *Prog. Polym. Sci.* **2000**, *25*, 711−779.

(5) Schacher, F.; Ulbricht, M.; Müller, A. H. Self-Supporting, Double Stimuli-Responsive Porous Membranes From Polystyrene-block-poly (N, N-dimethylaminoethyl methacrylate) Diblock Copolymers. *Adv. Funct. Mater.* **2009***, 7*, 1040-1045.

(6) Zhang, H.; Cooper, A. I. Synthesis and applications of emulsion-templated porous materials. *Soft Matter* **2005***, 2*, 107-113.

(7) Livshin, S. and Silverstein, M. S. Crystallinity and cross-linking in porous polymers synthesized from long side chain monomers through emulsion templating. *Macromolecules* **2008**, *41*, 3930-3938.

(8) Pierre, S. J.; Thies, J. C.; Dureault, A.; Cameron, N. R.; van Hest, J. C.; Carette, N.; Michon, T.; Weberskirch, R. Covalent enzyme immobilization onto photopolymerized highly porous monoliths. *Adv. Mater.* **2006**, *18*, 1822-1826.

(9) Martín, C. F.; Stöckel, E. V.; Clowes, R.; Adams, D. J.; Cooper, A. I.; Pis, J. J.; Rubiera, F.; Pevida, C. Hypercrosslinked organic polymer networks as potential adsorbents for pre-combustion CO_2 capture. *J. Mater. Chem.* **2011**, *21*, 5475-5483.

(10) Trewin, A.; Willock, D. J.; Cooper, A. I. Atomistic simulation of micropore structure, surface area, and gas sorption properties for amorphous microporous polymer networks. *The J. Mater. Chem. C.* **2008**, *112*, 20549-20559.

(11) Makhseed, S.; Samuel, J. Hydrogen adsorption in microporous organic framework polymer. *Chem Comm*. **2008**, *36*, 4342-4344.

(12) Budd, P. M.; Msayib, K. J.; Tattershall, C. E.; Ghanem, B. S.; Reynolds, K. J.; McKeown, N. B.; Fritsch, D. Gas separation membranes from polymers of intrinsic microporosity. *J Membr Sci.* **2005**, *251*, 263-269.

(13) Rose, M.; Klein, N.; Senkovska, I.; Schrage, C.; Wollmann, P.; Böhlmann, W.; Böhringer, B.; Fichtner, S.; Kaskel, S. A new route to porous monolithic organic frameworks via cyclotrimerization. *J. Mater. Chem*. **2011**, *21*, 711-716.

(14) Svec, F. Porous polymer monoliths: amazingly wide variety of techniques enabling their preparation. *J. Chromatogr. A*. **2010**, *1217*, 902-924.

(15) Cai, Y.; Chen, Y.; Hong, X.; Liu, Z.; Yuan, W. Porous microsphere and its applications. *Int. J. Nanomed*. **2013**, *8*, 1111.

(16) Coutinho, F. M.; Neves, M. A. F. S.; Dias, M. L. Porous structure and swelling properties of styrene-divinylbenzene copolymers for size exclusion chromatography. *J. Appl. Polym. Sci.* **1997**, *65*, 1257-1262.

(17) Okubo, M.; Konishi, Y.; Sebki, S.; Minami, H. Preparation of nonspherical polymer particles by spraying aqueous dispersions of hydrophobic solvent droplets into methanol. *Colloid Polym. Sci*. **2002**, *280***,** 765–769.

(18) Li, C.; Zhang, X.; Cao, Z. Triangular and Fibonacci number patterns driven by stress on core/shell microstructures. *Science* **2005**, *309*, 909–911.

(19) Utada, A. S.; Lorenceau, E.; Link, D. R.; Kaplan, P. D.; Stone, H. A.; Weitz, D. A. Monodisperse double emulsions generated from a microcapillary device. *Science* **2005**, *308*, 537–541.

(20) Rhutesh K. S.; Shum, H. C.; Rowat, A. C.; Lee, D.; Agresti, J. J.; Utada, A. S.; Chua, L. Y.; Kim, J. W.; Nieves, A. F.; Martinez, C. J.; Weitz, D. A. Designer emulsions using microfluidics, *Materials Today* **2008**, *11*, No 4, 18-27.

(21) Wang, W.; Xie, R.; Ju, X. J.; Luo, T.; Liu, L.; Weitz, D. A.; Chu, L. Y. Controllable microfluidic production of multicomponent multiple emulsions. *Lab Chip* **2011**, *11*, 1587–1592.

(22) Nabavi, S. A.; Vladisavljevic´, G. T.; Gu, S.; Ekanem, E. E. Double emulsion production in glass capillary microfluidic device: parametric investigation of droplet generation behaviour. *Chem. Eng. Sci.* **2015**, *130*, 183–196.

(23) Nabavi, S. A.; Vladisavljevic´, G. T.; Manovic, V. Mechanisms and control of single-step microfluidic generation of multi-core double emulsion droplets. *Chem. Eng. J*. **2017**, *322*, 140 -148.

(24) Okushima, S.; Nisisako, T.; Torii, T.; Higuchi, T. Controlled production of monodisperse double emulsions by two-step droplet breakup in microfluidic devices. *Langmuir* **2004**, *20*, 9905–9908.

(25) Kim, S. H.; Weitz, D. A. One-step emulsification of multiple concentric shells with capillary microfluidic devices. *Angew. Chem. Int. Ed. Engl.* **2011**, *123*, 8890–8893.

(26) Nisisako, T.; Okushima, S.; Torii, T. Controlled formulation of monodisperse double emulsions in a multiple-phase microfluidic system. *Soft Matter* **2005**, *1*, 23–27.

(27) Abate, A. R.; Thiele, J.; Weitz, D. A. One-step formation of multiple emulsions in microfluidics. *Lab Chip* **2011**, *11*, 253–258.

(28) Vladisavljević, G. T.; Al Nuumani, R.; Nabavi, S. Microfluidic Production of Multiple Emulsions. *Micromachines* **2017**, *8*, 75.

(29) Gokmen, M. T.; Dereli, B.; De Geest, B. G.; Du Prez, F. E. Complexity from simplicity: Unique polymer capsules, rods, monoliths, and liquid marbles prepared via HIPE in microfluidics. *Part. Part. Syst. Char*. **2013**, *30*, 438-444.

(30) Gong, X.; Wen, W.; Sheng, P. Microfluidic Fabrication of Porous Polymer Microspheres: Dual Reactions in Single Droplets. *Langmuir* **2009**, *25*, 7072–7077.
(31) Wang, B.; Prinsen, P.;Wang, H.; Bai, Z.; Wang, H.; Luque, R.; Xuan, J. Macroporous Materials: Microfluidic Fabrication, Functionalization and Applications. *Chem. Soc. Rev*. **2017**, *46*, 855-914.
(32) Zhang, M. J.; Wang, W.; Yang, X. L.; Ma, B.; Liu, Y. M.; Xie, R.; Ju, X. J.; Liu, Z.; Chu, L. Y. Uniform microparticles with controllable highly interconnected hierarchical porous structures, *ACS Appl. Mater. Interfaces* **2015**, *7*, 13758-13767.
(33) Wang, J.; Cheng, Y.; Yu, Y.; Fu, F.; Chen, Z.; Zhao, Y.; Gu, Z. Microfluidic Generation of Porous Microcarriers for Three-Dimensional Cell Culture. *ACS Appl. Mater. Interfaces* **2015***, 7*, 27035-27039.
(34) Liu, K.; Ding, H. J.; Liu, J.; Chen, Y.; Zhao, X. Z. Shape-controlled production of biodegradable calcium alginate gel microparticles using a novel microfluidic device. *Langmuir* **2006***, 22*, 9453-9457.
(35) Dendukuri, D.; Pregibon, D. C.; Collins, J.; Hatton, T. A.; Doyle, P. S. Continuous-flow lithography for high-throughput microparticle synthesis. *Nature Materials* **2006***, 5*, 365-369.
(36) Baah, D.; Tinger, J.; Bean, K.; Walker, N.; Britton, B.; Floyd-Smith, T. Microfluidic synthesis and post processing of non-spherical polymeric microparticles. *Microfluidics and Nanofluidics* **2012***, 12*, 657-662.
(37) Hakimi, N.; Tsai, S. S.; Cheng, C. H.; Hwang, D. K. One-step two-dimensional microfluidics-based synthesis of three-dimensional particles. *Advanced Materials* **2014***, 26*(9), 1393-1398.
(38) Donev, A.; Cisse, I.; Sachs, D.; Variano, E. A.; Stillinger, F. H.; Connelly, R.; Torquato, S.; Chaikin, P. M. Improving the density of jammed disordered packings using ellipsoids. *Science* **2004**, *303*, 990-993.
(39) Yamamoto, S.; Matsuoka, T. Viscosity of dilute suspensions of rodlike particles: A numerical simulation method. *J. Chem. Phys.* **1994**, *100*, 3317-3324.
(40) Hwang, D. K.; Dendukuri, D.; Doyle, P. S. Microfluidic-based synthesis of non-spherical magnetic hydrogel microparticles. *Lab Chip.* **2008**, *8*, 1640-1647.
(41) Gupta, S.; Zhang, Q.; Emrick, T.; Russell, T. P. "Self-corralling" nanorods under an applied electric field. *Nano Lett*. **2006**, *6*, 2066-2069.
(42) Glotzer, S. C.; Solomon, M. J. Anisotropy of building blocks and their assembly into complex structures. *Nat. Mater.* **2007**, *6*, 557-562.
(43) Shum, H. C.; Abate, A. R.; Lee, D.; Studart, A. R.; Wang, B.; Chen, C. H.; Thiele, J.; Shah, R. K.; Krummel, A.; Weitz, D. A. Droplet microfluidics for fabrication of non-spherical particles. *Macromol. Rapid Commun*. **2010**, *31*,108-118.
(44) Lee, S.; Abbaspourrad, A.; Kim, S. H. Nonspherical double emulsions with multiple distinct cores enveloped by ultrathin shells. *ACS Appl. Mater. Interfaces* **2014**, *6*, 1294–1300.
(45) Lee, S. D.; Weitz, D. A. Nonspherical colloidosomes with multiple compartments from double emulsions, *Small* **2009**, *5*, 1932–1935.

(46) Zhang, W.; Thompson, K. E.; Reed, A. H.; Beenken, L. Relationship between packing structure and porosity in fixed beds of equilateral cylindrical particles. *Chem. Eng. Sci.* **2006**, *61*, 8060 -8074.
(47) Shen, S.; Gu, T.; Mao, D.; Xiao, X.; Yuan, P.; Yu, M.; Xia, L.; Ji, Q.; Meng, L.; Song, W.; Yu, C.; Lu, G. Synthesis of Hard Magnetic Ordered Mesoporous Co_3O_4/$CoFe_2O_4$ Nanocomposites. *Chem. Mater*. **2012**, *24*, 230–235.
(48) Dugyala, V. R.; Daware, S. V.; Basavaraj, M. G. Shape anisotropic colloids: synthesis, packing behavior, evaporation driven assembly, and their application in emulsion stabilization. *Soft Mater*. **2013**, *9*, 6711–6725.
(49) Doshi, N.; Mitragotri, S. Macrophages recognize size and shape of their targets. *PLoS One* **2010**, *5*, e10051.
(50) Fish, M. B.; Thompson, A. J.; Fromen, C. A.; Eniola-Adefeso, O. Emergence and Utility of Nonspherical Particles in Biomedicine. *Ind. Eng. Chem. Res.* **2015**, *54*, 4043–4059.
(51) Champion, J. A.; Katare, Y. K.; Mitragotri, S. Particle shape: a new design parameter for micro- and nanoscale drug delivery carriers. *Journal of controlled release* **2007***, 121*, 3-9.
(52) Nisisko, T.; Ando, T.; Hatsuzawa, T. Capillary-assisted fabrication of biconcave polymeric microlenses from microfluidic ternary emulsion droplets. *Small* **2014**, *10*(24), 5116-5125.
(53) Glotzer, S. C.; Solomon, M. J. Anisotropy of building blocks and their assembly into complex structures. *Nature Materials* **2007***, 6*(8), 557-562.
(54) Sacanna, S.; Pine, D. J. Shape-anisotropic colloids: Building blocks for complex assemblies. *Current Opinion in Colloid & Interface Science* **2011***, 16*(2), 96-105.
(55) Xu, S.; Nie, Z.; Seo, M.; Lewis, P.; Kumacheva, E.; Stone, H. A.; Garstecki, P.; Weibel, D. B.; Gitlin, I.; Whitesides, G. M. Generation of monodisperse particles by using microfluidics: control over size, shape, and composition. *Angewandte Chemie* **2005**, *117*, 734-738.
(56) Kim, S. H.; Hwang, H.; Lim, C. H.; Shim, J. W.; Yang, S. M. Packing of emulsion droplets: structural and functional motifs for multi-cored microcapsules. *Adv. Funct. Mater*. **2011**, *21*, 1608–1615.
(57) Khan, I. U.; Stolch, L.; Serra, C. A.; Anton, N.; Akasov, R.; Vandamme, T. F. Microfluidic conceived pH sensitive core–shell particles for dual drug delivery. *Int. J. Pharm.* **2015**, *478*, 78-87.
(58) Fleischmann, E. K.; Liang, H. L.; Kapernaum, N.; Giesselmann, F.; Lagerwall, J.; Zentel, R. One-piece micropumps from liquid crystalline core-shell particles. *Nat. Commun.* **2012**, *3*, 1178.
(59) Abate, A. R.; Weitz, D. A. High-order multiple emulsions formed in poly (dimethylsiloxane) microfluidics. *Small* **2009**, *5*, 2030-2032.
(60) Cameron, N. R., Sherrington, D. C., Albiston, L., Gregory, D. P. Study of the formation of the open-cellular morphology of poly (styrene/divinylbenzene) polyHIPE materials by cryo-SEM. *Colloid Polym. Sci.* **1996**, *274*, 592-595.
(61) Sajjadi, S.; Zerfa, M.; Brooks, B. W. Morphological Change in Drop Structure with Time for Abnormal Polymer/Water/Surfactant Dispersions. *Langmuir* **2000**, *16*, 10015–10019.

(62) Josephides, D. N.; Sajjadi, S. Microfluidic method for creating monodisperse viscous single emulsions via core-shell templating. *Microfluid Nanofluid* **2015**, *18*, 383 -390.

(63) Chaurasia, A. S.; Sajjadi, S. Transformable Bubble-filled Alginate Microfibers via Vertical Microfluidics. *Lab Chip* **2019**, *19*, 851-863.

(64) Chaurasia, A. S.; Sajjadi, S. Flexible asymmetric encapsulation for dehydration-responsive Hybrid microfibers, *Small* **2016**, *2*, 4146-4155.

(65) Sujit, S. D.; Abbaspourrad, A.; Amstad, E.; Fan, J.; Kim, S. H.; Romanowsky, M.; Shum, H. C.; Sun, B.; Utada, A. S.; Windbergs, M.; Zhou, S.; Weitz, D. A. 25th Anniversary Article: Double Emulsion Templated Solid Microcapsules: Mechanics And Controlled Release. *Adv. Mater.* **2014**, *26*, 2205–2218.